International Journal of Minerals, Metallurgy and Materials
Volume 26, Number 10, October 2019, Page 1231
https://doi.org/10.1007/s12613-019-1868-8

Growth behavior of the magnetite phase in the reduction of hematite via a fluidized bed

Jian-wen Yu[1,2], *Yue-xin Han*[1], *Yan-jun Li*[1], *and Peng Gao*[1]

1) School of Resources and Civil Engineering, Northeastern University, Shenyang 110819, China

2) State Key Laboratory of Mineral Processing, Beijing General Research Institute of Mining & Metallurgy Group, Beijing 102628, China

(Received: 31 January 2019; revised: 13 May 2019; accepted: 3 June 2019)

Abstract: To understand the formation and growth mechanism of the magnetite phase during the fluidized reduction of hematite, a high-purity hematite ore was isothermally reduced using a 20vol% CO−80vol% CO_2 gas mixture in a micro-fluidized bed to examine the process of the selective conversion of hematite to magnetite. The micro-structural characteristics of the magnetite phase were investigated using scanning electron microscopy (SEM) and the Brunauer, Emmett, and Teller (BET) method, and the thickness of the magnetite layer was measured and evaluated using statistical analysis. The experimental results showed that the fresh magnetite nuclei were dense needles of different lengths, and the original hematite grains became porous after complete reduction to the magnetite phase. The thickness of the magnetite layer increased with an increase in reduction temperature and reduction time. The growth kinetics of the magnetite layer was investigated, and the value of the activation energy E was estimated to be 28.33 kJ/mol.

Keywords: hematite ore; fluidized bed; suspension magnetization roasting; magnetite; growth kinetics

1. Introduction

In the 21st century, steel remains an irreplaceable raw material for human activities as well as a measure of national strength and the industrial level of a country [1−2]. With the rapid development of the steel industry worldwide, the highest-quality iron ore resources have been gradually depleted, and refractory low-grade iron ores such as siderite, limonite, and hematite have become the main sources of raw materials for the steel industry [3−4]. These refractory iron ores are commonly characterized by low iron content and the ultra-fine grain size of the iron minerals. Thus, conventional beneficiation methods, including gravity concentration, magnetic separation, and flotation, are less effective in producing a qualified iron concentrate from such refractory iron ores [5−10]. In order to utilize these materials, fluidized magnetization roasting followed by magnetic separation has been recently proposed to recover iron from refractory iron ores. In this method, weakly magnetic iron minerals, such as hematite, siderite, and limonite are selectively converted to ferromagnetic magnetite, which is subsequently liberated by grinding and easily separated from the gangue minerals by magnetic separation [11−15].

Many excellent studies of the fluidized magnetization roasting of refractory iron ores have been carried out. Boehm *et al.* [16] investigated the selective magnetizing flash roasting of siderite in an oxidizing atmosphere on a pilot plant scale. An iron recovery of 80%–92% with a mass yield of 67%–75% magnetic concentrate was achieved, indicating that the siderite was successfully transformed to magnetite. Li and Zhu [17] studied the magnetic properties and phase transformation of a low-grade hematite ore from Tangshan, China via fluidized bed magnetization roasting, and obtained a magnetic concentrate assaying 62.5% Fe with a recovery rate of 91.1%. Li *et al.* [18] used vibrating sample magnetometer (VSM), X-ray diffraction (XRD), and Mossbauer spectroscopy methods to analyze the magnetic properties and phase conversion of an oolitic hematite ore after fluidized reduction roasting with a H_2/N_2 gas mixture. The results showed that the hematite within the ore could be rapidly reduced to magnetite, thereby significantly enhancing magnetization and magnetic susceptibility. Yu and

Corresponding authors: Yan-jun Li E-mail: liyanjun@mail.neu.edu.cn; Peng Gao E-mail: gaopeng@mail.neu.edu.cn

Qi [19] examined the feasibility of flash magnetizing roasting to process several representative refractory iron ores and discussed the flash magnetizing roasting mechanism. The results indicated that hematite, limonite, and siderite could be selectively reduced to magnetite within 60 s via flash magnetizing roasting due to its efficient heat and mass transfer. Feilmayr *et al.* [20] carried out research on the reduction behaviors of Mt. Newman hematite ore from Western Australia, which contains both limonite and martite, in a fluidized reactor between 623 and 873 K and found that the phase interface reaction was controlled by the chemical reaction rate between 673 and 773 K, and its activation energy was 91 kJ/mol. Additionally, the thickness of the dense magnetite layers was linearly proportional to the reduction time. In our previous work [21−27], we found that hematite and siderite could be selectively reduced to magnetite after fluidized magnetization roasting pretreatment, and the mechanism and kinetics of the reduction of hematite to magnetite in a laboratory-scale fluidized bed were also examined. In fact, the grain size of the magnetite phase plays a vital role in the subsequent magnetic separation process, because coarse magnetite grains can be more easily liberated and recovered from the gangue minerals. However, the formation and growth behavior of the magnetite phase in fluidized magnetization roasting are not clear. Thus, it is necessary to carry out the relevant basic research.

To better understand the formation and growth of the magnetite phase, experiments were conducted with a high-purity hematite ore at temperatures from 773 to 873 K in a micro-fluidized bed. A 20vol% CO−80vol% CO_2 gas mixture in thermodynamic equilibrium with the magnetite was used as the reductant. The formation process and microstructure of the magnetite phase were studied using scanning electron microscopy (SEM) and the Brunauer, Emmett, and Teller (BET) method. The size of the magnetite phase in the reduced hematite ore was determined using a reflected-light microscope, and the growth kinetics of the magnetite phase were also analyzed.

2. Experimental

The raw material used in present work was pure hematite ore with an average particle size of 70 μm. The hematite ore was taken from Hainan Province, China. The iron content of the sample was 65.44wt%, and the content of the main impurity, silica, was 4.11wt%, indicating that the purity of the hematite in this ore was 93.5%.

An SEM image of the ore sample is shown in Fig. 1; the image demonstrated that the size of the particles was relatively uniform. The uniform size of the original particles confirmed the representativeness of the thickness measurements of the magnetite phase generated by fluidized bed roasting. A mixture of carbon monoxide and carbon dioxide gas (1:4 in volume ratio) was used as the reducing and fluidizing agent, and nitrogen was used as a protective gas.

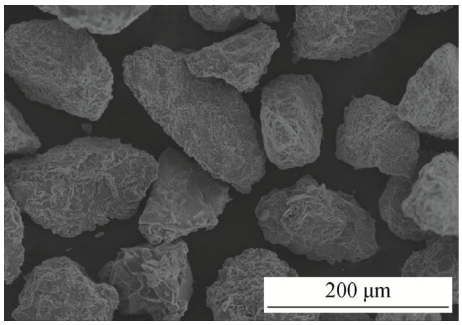

Fig. 1. SEM images of the hematite sample used.

A 5.0 g iron ore sample was placed on a perforated quartz plate bed and isothermally roasted in a vertical tube furnace under pre-set experimental conditions. The roasted samples were then cooled to room temperature under a nitrogen atmosphere. After cooling, the roasted samples were removed from the furnace and characterized using various methods. The detailed experimental procedures are described in our previous work [23].

To obtain insight into the formation and growth behaviors of the magnetite phase during the fluidized reduction of hematite ore, the original hematite ore and the fluidized reduction products were first mounted in a Bakelite block and polished to expose the inner surfaces of the particles. The polished samples were then investigated using SEM (S-3400N; Hitachi, Ltd., Tokyo, Japan) and optical microscopy (Leica DM4 P, Germany). The line segment method was used to directly measure the thickness of the magnetite layer using optical microscopy (as shown in Fig. 2), and the growth kinetics was analyzed based on the measurement data. The surface area and pore size measurements of the raw hematite ore and the roasted sample were carried out by means of the BET (liquid N_2) method, using an ASAP 2020-Physisorption analyzer (Micromeritics Instrument Corp., USA).

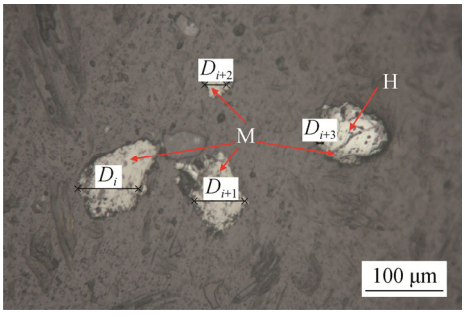

Fig. 2. Size measurement for magnetite layers in reduction samples (H—hematite; M—magnetite).

3. Results and discussion

3.1. Formation of the magnetite phase

Fig. 3 shows the XRD patterns of the original hematite ore and the samples reduced at 873 K. The raw hematite ore was mainly composed of hematite and a small amount of quartz, indicating that it was relatively pure. After 2 min of roasting, the characteristic peaks of the new magnetite phase appeared, and the intensity of the characteristic peaks of hematite decreased, revealing that some of the hematite had already been converted to magnetite. When the reduction time was extended to 7 min, the characteristic peaks of hematite disappeared and no peaks characteristic of metallic iron or wüstite were observed, indicating that the hematite had been completely reduced to magnetite without over-reduction.

The original hematite ore and the reduced samples were then examined using SEM; the resulting images are shown in Fig. 4. As shown in Fig. 4(a), the polished hematite surface was dense and smooth without micro-cracks or pores. After 2 min of roasting, the new magnetite phase had begun to form at the edge of the particle and exhibited a porous structure, as shown in Fig. 4(b). These observations indicated that the reducing gas CO first reacted with the edges of the dense hematite particle to form magnetite. After 7 min of reduction, the number of micro-cracks or pores had increased, and the hematite particle had been completely transformed into magnetite (Fig. 4(c)). As shown in Fig. 4(d), the newly generated magnetite exhibited a dense needle morphology with an average length of 10 μm and an average diameter of 1 μm; this dense needle-like magnetite then aggregated to form porous magnetite particles.

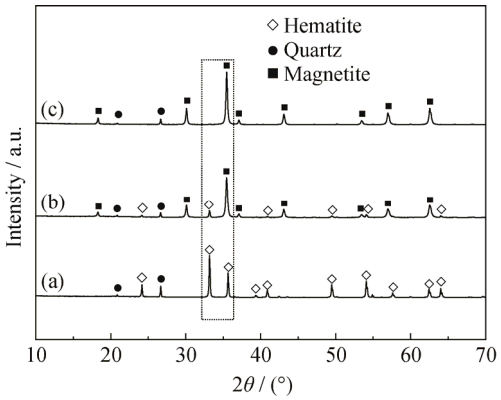

Fig. 3. XRD patterns of the original hematite ore and the samples reduced at 873 K: (a) raw hematite ore; (b) roasting for 2 min; (c) roasting for 7 min.

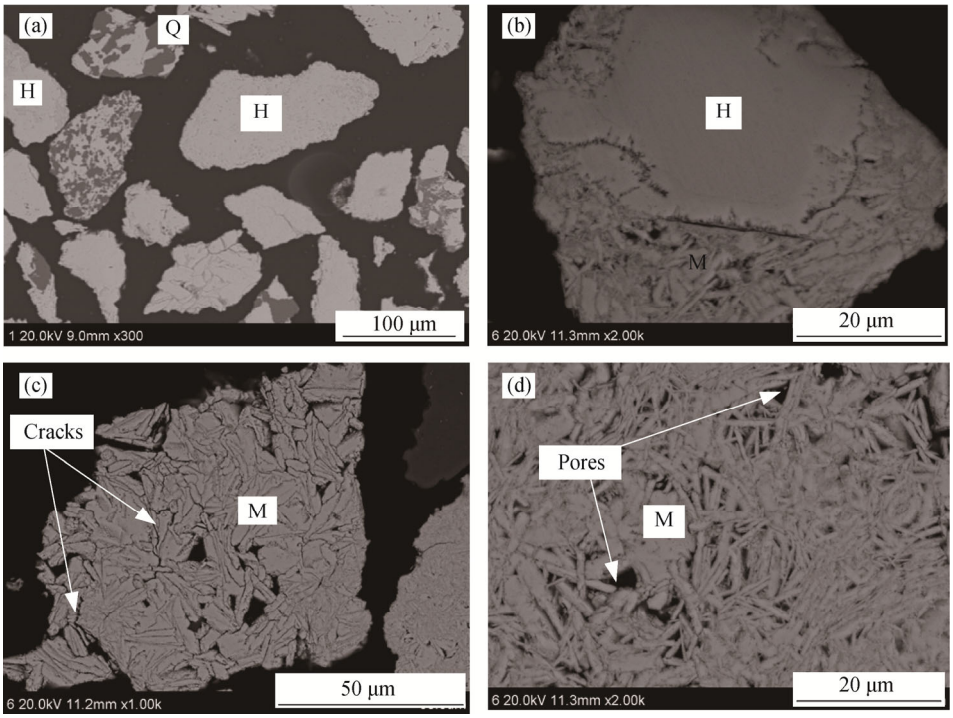

Fig. 4. SEM images of the original hematite ore and the samples reduced at 873 K for different times: (a) raw hematite ore; (b) 2 min; (c, d) 7 min (Q—quartz; H—hematite; M—magnetite).

Based on the above analyses, the magnetite formation process can be deduced. Fresh needle-shaped magnetite nuclei were formed at the edges of the original hematite particle. The Fe^{2+} produced by the reaction was transported to the tip of the needle-shaped magnetite nuclei by diffusion, which promoted the growth of the magnetite nuclei. Mi-

cro-cracks were easily and randomly formed at the interface between the magnetite, which has a cubic crystal structure, and hematite, which has a hexagonal structure, due to their different crystal structures. If a micro-crack occurred at the tip of a needle-shaped magnetite nucleus, the diffusion path of Fe^{2+} to the tip was destroyed, and the growth of the needle-shaped magnetite nucleus stopped. Thus, acicular magnetite was generated with different lengths, as shown in Fig. 4(d). With further reaction time, the sizes of the needle-like magnetite nuclei increased and aggregated to form a porous magnetite particle.

3.2. Growth kinetics of the magnetite layers

As discussed above, measurements of the apparent thickness of the magnetite layer generated at different roasting conditions were carried out using optical microscopy. To provide a quantitative and scientific description, the average thickness of the magnetite layer for a given roasting condition was calculated using the following equation:

$$D = \frac{1}{N}\sum_{i=1}^{N} D_i \tag{1}$$

where D is the average thickness of the magnetite layer, D_i is the thickness of the i-th magnetite layer, and N is the total number of original hematite particles (N = 100). The average thickness of the magnetite layers under different roasting conditions is illustrated in Fig. 5.

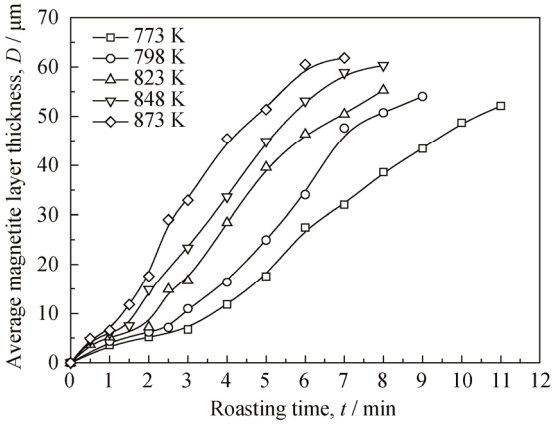

Fig. 5. Average thickness of the magnetite layers under different roasting conditions.

As shown in Fig. 5, the average thickness of the magnetite layer clearly increased with an increase in roasting temperature and time. For example, when the roasting temperature was increased from 773 to 873 K for a roasting time of 4 min, the magnetite layer thickness increased from 11.8 to 45.4 μm. The results showed that the magnetite phase grew into large-sized grains (layers) with an increase in roasting temperature or time until the hematite was completely reduced to magnetite.

Isothermal grain (product layer) growth kinetics have been intensively studied, and can be expressed as the following classical relationship [28–29]:

$$D^{1/n} - D_0^{1/n} = K \cdot t \tag{2}$$

where D is the average grain size, D_0 is the grain size at t = 0, t is the roasting time, n is the time exponent, and K is the rate constant.

The rate constant K in Eq. (2) can be calculated using the following Arrhenius equations:

$$K = K_0 \cdot \exp\left(-\frac{E}{RT}\right) \quad \text{or} \quad \ln K = \ln K_0 - \frac{E}{R}\cdot\frac{1}{T} \tag{3}$$

where K_0 is the pre-exponential constant, R is the gas constant, T is the absolute temperature, and E is the apparent activation energy. At t = 0, no magnetite is generated. Thus, D_0 is 0. By substituting Eq. (3) into Eq. (2), the average grain size can be expressed as the following equations:

$$D^{1/n} = K_0 \exp\left(-\frac{E}{RT}\right)\cdot t \quad \text{or} \quad \ln D = n\left(\ln K_0 - \frac{E}{RT} + \ln t\right) \tag{4}$$

Clearly, the value of n can be readily obtained by plotting ln$D$ against ln$t$; n is equal to the slope of the fitted line; The plots of ln$D$ vs. ln$t$ are shown in Fig. 6, and the linear fitting results demonstrated good linearity with a high correlation coefficient R^2, indicating that the values of n were reliable. Thus, the average value of n was determined to be 1.1673.

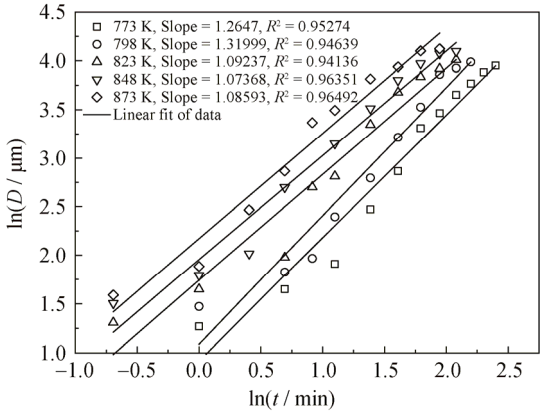

Fig. 6. Plots of ln$D$ vs. ln$t$ calculated from the measured magnetite layer thicknesses using Eq. (4).

The value of K can be obtained by plotting $D^{1/n}$ against t, and the E and K_0 values can then be obtained from the slope and intercept of the linear fitting of ln$K$ vs. 1/T, respectively. The linear fittings of $D^{1/n}$ (n = 1.1673) against t are presented in Fig. 7.

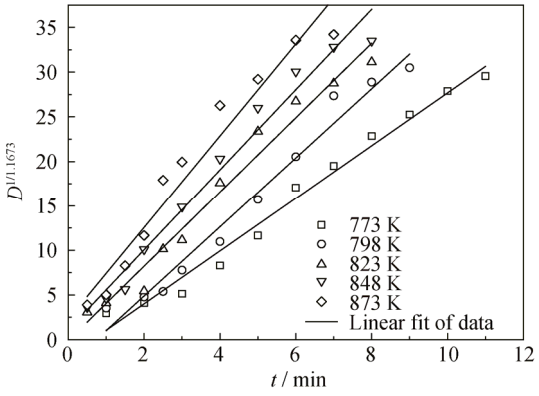

Fig. 7. Plots of $D^{1/n}$ (n = 1.1673) vs. t calculated from the measured magnetite layer thicknesses using Eq. (2).

As shown in Fig. 7, the linear correlation coefficients between $D^{1/n}$ and t at different temperatures are favorable. Correspondingly, the K values were obtained from the slopes of the linear regressions.

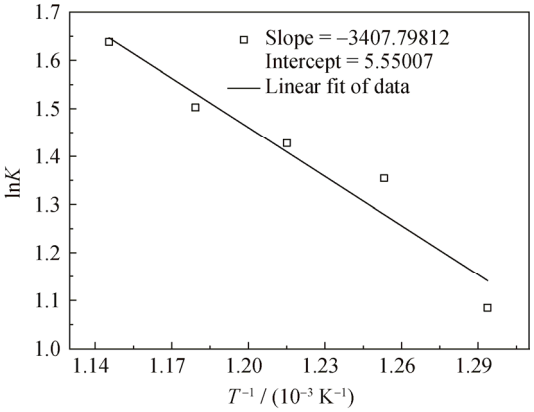

Fig. 8. Plots of ln$K$ vs. 1/T calculated from the measured magnetite layer thicknesses using Eq. (3).

Fig. 8 depicts the plot of ln$K$ vs. 1/T , which showed good linearity. From the slope and intercept of the linear fitting of ln$K$ vs. 1/T, the values of E and K_0 were calculated to be 28.33 kJ·mol^{-1} and 257.26, respectively. Thus, the growth model for the magnetite particles (layers) in the fluidized reduction of hematite was derived using the following equation:

$$D^{1/1.1673} = 257.26 \exp\left(-\frac{28330}{RT}\right) \cdot t \quad (5)$$

Fig. 9 shows a graphical comparison of the thickness of the magnetite layer predicted using Eq. (5) with the experimental data. The theoretically modeled values did not coincide exactly with the experimentally measured ones. However, the modeled magnetite layer thickness points were evenly scattered around the $y = x$ line, which shows the similarity between the experimentally measured and modeled values. Thus, the proposed growth kinetics model can be used successfully to describe the growth of the magnetite layers (particles) during the fluidized reduction of hematite.

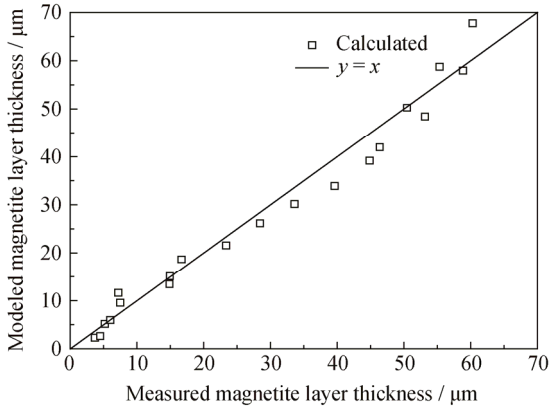

Fig. 9. Comparison of experimental data with growth model.

3.3. Reduction model of hematite to magnetite

Fig. 10 presents the SEM images of samples reduced at 873 K for different times. As shown in Fig. 10(a), very few particles contained traces of magnetite early in the reduction. As the reduction time increased, an increasing amount of magnetite was generated. This magnetite eventually aggregated to form a porous layer, but the initial magnetite nuclei were dense needles. The needle-like magnetite nuclei surrounded the hematite core with interstitial pores, as shown in Figs. 10(b) and 10(c). These pores were randomly interconnected and accessible for the transport of the reducing gas, CO. These observations suggest that the reducing gas could successfully pass through the porous magnetite layer. Therefore, oxygen removal mainly occurred at the external surfaces of the magnetite nuclei and the unreacted hematite during the reduction.

The needle-like magnetite nuclei randomly grew from the external surface of the hematite to the inner core, and were distributed in grains with a dendritic structure, as shown in Figs. 10(c) and 10(d). Thus, the magnetite layers grew gradually from the outer surface of hematite to the inner core until the hematite grain was completely converted to magnetite.

The surface area and porosity analyses of the raw hematite ore and the sample roasted at 873 K for 7 min indicated that the BET surface area increased from 0.6693 to 1.4751 m^2/g and the pore size increased from 15.89 to 54.89 nm after reduction roasting, indicating that the original hematite particles became porous after full conversion to the magnetite phase, which was in good agreement with the above analyses.

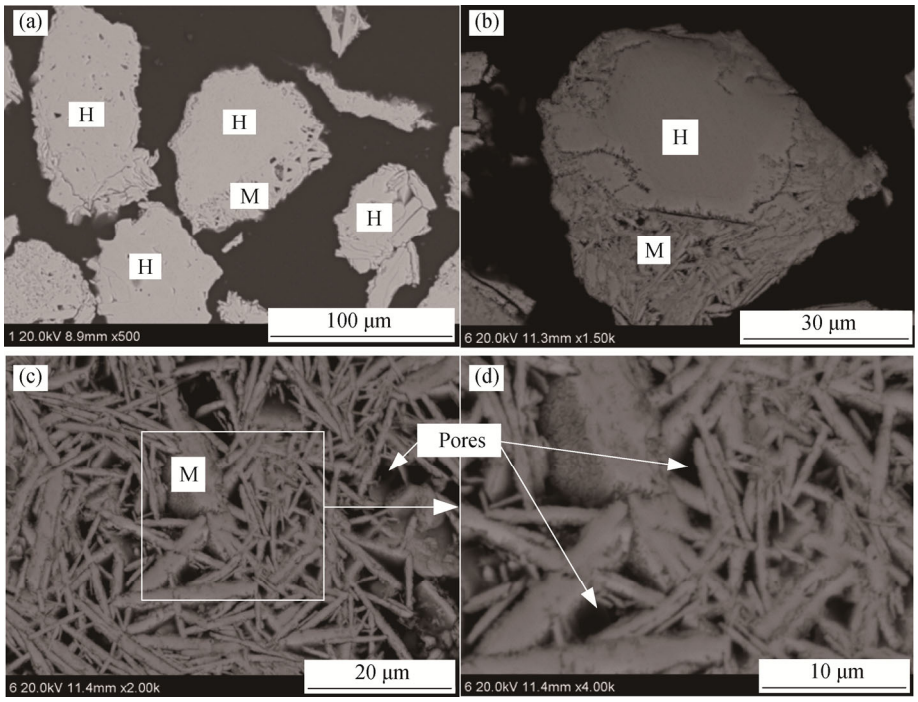

Fig. 10. SEM images of the samples reduced at 873 K for different times: (a) 0.5 min; (b) 2 min; (c, d) 7 min (H—hematite; M—magnetite).

Based on the above analyses, the main process of the formation and growth of the magnetite phase can be described as follows: The reducing agent CO diffused to the external surface of the original hematite crystal, removing an oxygen atom and freeing two electrons. The electrons reduced Fe^{3+} to Fe^{2+}; the electrons and generated ferrous ions then diffused into the hematite core through the magnetite layer, where fresh magnetite was generated through lattice re-construction [20,30]. Meanwhile, the reducing gas, CO, entered the newly formed micropores and eventually reached the fresh surface of the hematite grain to participate in the reduction of hematite to magnetite, i.e., the reducing gas, CO, could successfully permeate through the porous magnetite layer to react with the fresh hematite. Thus, oxygen removal might occur on the outer surface of the magnetite layer or on the fresh inner surface of the hematite grain. Finally, the whole hematite grain was completely reduced to magnetite. The overall process of magnetite formation and growth during the fluidized reduction of hematite is illustrated in Fig. 11.

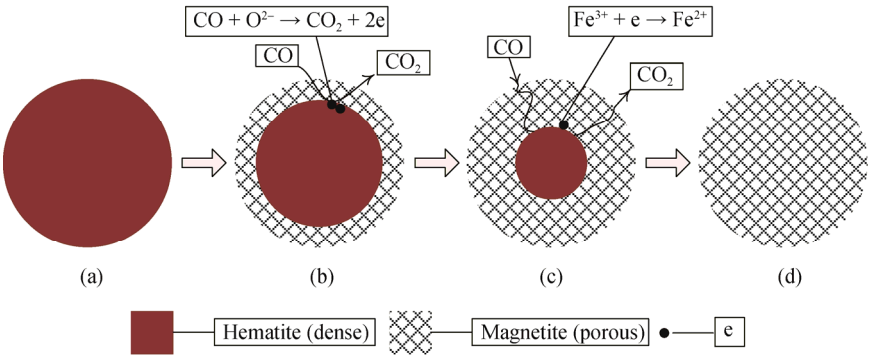

Fig. 11. Schematic diagram of the formation and growth of the magnetite phase: (a) before reaction; (b) initial stage of reaction; (c) latter stage of reaction; (d) after reaction.

4. Conclusions

In this study, the formation and growth kinetics of the magnetite phase during the reduction of hematite with 20vol% CO−80vol% CO_2 in a micro-fluidized bed reactor were investigated. The major findings are as follows.

(1) The fresh magnetite nuclei were dense needles with different lengths, and preferentially formed at the edges of original hematite particles. The original hematite grains became porous after complete reduction to magnetite.

(2) The thickness of the magnetite layer increased with an increase in reduction temperature and roasting time. The value of the activation energy E for the growth of the magnetite layer was estimated to be 28.33 kJ/mol.

(3) The reducing gas could permeate through the porous magnetite layer. Thus, oxygen removal could occur on the outer surface of the magnetite layer or on the fresh inner surface of the hematite grain during the reduction.

Acknowledgements

This work was financially supported by the National Science Foundation of China (Nos. 51734005 and 51674065), the China Postdoctoral Science Foundation (No. 2018M631812), and Open Foundation of State Key Laboratory of Mineral Processing, Beijing General Research Institute of Mining & Metallurgy Group, China (No. BGRIMM-KJSKL-2019-09).

References

[1] Y.S. Sun, Y.X. Han, P. Gao, and J.W. Yu, Size distribution behavior of metallic iron particles in coal-based reduction products of an oolitic iron ore, *Miner. Process. Extr. Metall. Rev.*, 36(2015), No. 4, p. 249.

[2] J.W. Yu, Y.X. Han, Y.J. Li, P. Gao, and Y.S. Sun, Separation and recovery of iron from a low-grade carbonate-bearing iron ore using magnetizing roasting followed by magnetic separation, *Sep. Sci. Technol.*, 52(2017), No. 10, p. 1768.

[3] T.J. Chun, D.Q. Zhu, and J. Pan, Simultaneously roasting and magnetic separation to treat low grade siderite and hematite ores, *Miner. Process. Extr. Metall. Rev.*, 36(2015), No. 4, p. 223.

[4] L.Q. Luo, M. Chen, H.T. Yan, S.S. Cui, and Y.J. Zhang, Magnetic reduction roasting and magnetic separation of oolitic iron ore, *Chin. J. Proc. Eng.*, 14(2014), No. 4, p. 593.

[5] X.M. Luo, Y.F. Wang, S.M. Wen, M.Z. Ma, C.Y. Sun, W.Z. Yin, and Y.Q. Ma, Effect of carbonate minerals on quartz flotation behavior under conditions of reverse anionic flotation of iron ores, *Int. J. Miner. Process.*, 152(2016), p. 1.

[6] D. Li, W.Z. Yin, J.W. Xue, J. Yao, Y.F. Fu, and Q. Liu, Solution chemistry of carbonate minerals and its effects on the flotation of hematite with sodium oleate, *Int. J. Miner. Metall. Mater.*, 24(2017), No. 7, p. 736.

[7] X.M. Luo, W.Z. Yin, Y.F. Wang, C.Y. Sun, Y.Q. Ma, and J. Liu, Effect and mechanism of siderite on reverse anionic flotation of quartz from hematite, *J. Cent. South Univ.*, 23(2016), No. 1, p. 52.

[8] X.M. Luo, W.Z. Yin, Y.F. Wang, C.Y. Sun, Y.Q. Ma, and J. Liu, Effect and mechanism of dolomite with different size fractions on hematite flotation using sodium oleate as collector, *J. Cent. South Univ.*, 23(2016), No. 3, p. 529.

[9] S. Song, S. Lu, and A. Lopez Valdivieso, Magnetic separation of hematite and limonite fines as hydrophobic flocs from iron ores, *Miner. Eng.*, 15(2002), No. 6, p. 415.

[10] L.Q. Luo, J.S. Zhang, and Y.F. Yu, Recovering limonite from Australia iron ores by flocculation-high intensity magnetic separation, *J. Cent. South Univ. Technol.*, 12(2005), No. 6, p. 682.

[11] Q.S. Zhu and H.Z. Li, Status quo and development prospect of magnetizing roasting via fluidized bed for low grade iron ore, *CIESC J.*, 65(2014), No. 7, p. 2437.

[12] J.W. Yu, Y.X. Han, Y.J. Li, and P. Gao, Beneficiation of an iron ore fines by magnetization roasting and magnetic separation, *Int. J. Miner. Process.*, 168(2017), p. 102.

[13] X. Liu, Y. Yu, Z. Hong, Z. Peng, J. Li, Q. Zhao, Development and application of packaged technology for flash (fluidization) magnetizing roasting of refractory weakly magnetic iron ore, *Min. Metall. Eng.*, 37(2017), No. 2, p. 40.

[14] W. Chen, Y.F. Yu, Z. Feng, X. Lu, Q. Zhao, X. Liu, Six hundred thousand t/a refractory siderite flash magnetizing roasting complete sets technique and equipment, *Met. Mine*, 2017, No. 3, p. 54.

[15] Y.F. Yu and W. Chen, Application of flash magnetizing roasting technique in beneficiation of siderite and limonite, [in] *International Symposium on Project Management*, Shuyang, 2010, p. 13.

[16] A. Boehm, M. Boehm, and A. Kogelbauer, Neutrons for mineral processing–thermo diffractometry to investigate mineral selective magnetizing flash roasting, *Chem. Ing. Tech.*, 86(2014), No. 6, p. 883.

[17] Y. Li and T. Zhu, Recovery of low grade haematite via fluidised bed magnetising roasting: investigation of magnetic properties and liberation characteristics, *Ironmaking Steelmaking*, 39(2012), No. 2, p. 112.

[18] Y.J. Li, R. Wang, Y.X. Han, and X.C. Wei, Phase transformation in suspension roasting of oolitic hematite ore, *J. Cent. South Univ.*, 22(2015), No. 12, p. 4560.

[19] Y.F. Yu and C.Y. Qi, Magnetizing roasting mechanism and effective ore dressing process for oolitic hematite ore, *J. Wuhan. Univ. Technol.*, 26(2011), No. 2, p. 176.

[20] C. Feilmayr, A. Thurnhofer, F. Winter, H. Mali, and J. Schenk, Reduction behavior of hematite to magnetite under fluidized bed conditions, *ISIJ Int.*, 44(2004), No. 7, p. 1125.

[21] J.W. Yu, Y.X. Han, Y.J. Li, and P. Gao, Recovery and separation of iron from iron ore using innovative fluidized magnetization roasting and magnetic separation, *J. Min. Metall. B*, 54(2018), No. 1, p. 21.

[22] J.W. Yu, Y.X. Han, P. Gao, Y.J. Li, S. Yuan, and W.B. Li, An innovative methodology for recycling iron from magnetic preconcentrate of an iron ore tailing, *Physicochem. Prob. Miner. Process.*, 54(2018), p. 668.

[23] J.W. Yu, Y.X. Han, Y.J. Li, P. Gao, and W.B. Li, Mechanism

and kinetics of the reduction of hematite to magnetite with CO–CO_2 in a micro-fluidized bed, *Minerals*, 7(2017), No. 11, 209.

[24] J.W. Yu, Y.X. Han, Y.J. Li, and P. Gao, Recent advances in magnetization roasting of refractory iron ores: A technological review in the past decade, *Miner. Process. Extr. Metall. Rev.*, 2019. DOI: 10.1080/08827508.2019.1634565

[25] Y.S. Sun, X.R. Zhu, Y.X. Han, and Y.J. Li, Green magnetization roasting technology for refractory iron ore using siderite as a reductant, *J. Cleaner Prod.*, 206(2019), p. 40.

[26] X.L. Zhang, Y.X. Han, Y.S. Sun, and Y.J. Li, Innovative utilization of refractory iron ore via suspension magnetization roasting: A pilot-scale study, *Powder Technol.*, 352(2019), p. 16.

[27] X.L. Zhang, Y.X. Han, Y.S. Sun, Y. Lv, Y.J. Li, and Z.D. Tang, An novel method for iron recovery from iron ore tailings with pre-concentration followed by magnetization roasting and magnetic separation, *Miner. Process. Extr. Metall. Rev.*, 2019. DOI: 10.1080/08827508.2019.1604522

[28] G.W. Yang, X.J. Sun, Q.L. Yong, Z.D. Li, and X.X. Li, Austenite grain refinement and isothermal growth behavior in a low carbon vanadium microalloyed steel, *J. Iron Steel Res. Int.*, 21(2014), No. 8, p. 757.

[29] Y.S. Sun, Y.X. Han, Y.J. Li, and Y.F. Li, Formation and characterization of metallic iron grains in coal-based reduction of oolitic iron ore, *Int. J. Miner. Metall. Mater.*, 24(2017), No. 2, p. 123.

[30] M. Et-Tabirou, B. Dupré, and C. Gleitzer, Hematite single crystal reduction into magnetite with CO−CO_2, *Metall. Trans. B*, 19(1988), No. 2, p. 311.